

Stable photocurrent-voltage characteristics of perovskite single crystal detectors obtained by pulsed bias

Xin Liu(刘新), Zhi-Long Chen(陈之龙), Hu Wang(王虎), Wen-Qing Zhang(张雯清), Hao Dong(董昊), Peng-Xiang Wang(王鹏祥), and Yu-Chuan Shao(邵宇川)

Citation: Chin. Phys. B, 2024, 33 (**4**): 048101. DOI: 10.1088/1674-1056/ad23d7
Journal homepage: http://cpb.iphy.ac.cn; http://iopscience.iop.org/cpb

What follows is a list of articles you may be interested in

High-temperature continuous-wave operation of 1310 nm InAs/GaAs quantum dot lasers

Xiang-Bin Su(苏向斌), Fu-Hui Shao(邵福会), Hui-Ming Hao(郝慧明), Han-Qing Liu(刘汗青),Shu-Lun Li(李叔伦), De-Yan Dai(戴德炎), Xiang-Jun Shang(尚向军), Tian-Fang Wang(王天放),Yu Zhang(张宇), Cheng-Ao Yang(杨成奥), Ying-Qiang Xu(徐应强), Hai-Qiao Ni(倪海桥),Ying Ding(丁颖), and Zhi-Chuan Niu(牛智川)
Chin. Phys. B, 2023, 32 (**9**): 098103. DOI: 10.1088/1674-1056/acb491

Accurate determination of anisotropic thermal conductivity for ultrathin composite film

Qiu-Hao Zhu(朱秋毫), Jing-Song Peng(彭景凇), Xiao Guo(郭潇), Ru-Xuan Zhang(张如轩), Lei Jiang(江雷), Qun-Feng Cheng(程群峰), and Wen-Jie Liang(梁文杰)
Chin. Phys. B, 2022, 31 (**10**): 108102. DOI: 10.1088/1674-1056/ac6ee5

Suppression of ion migration in perovskite materials by pulse-voltage method

Xue-Yan Wang(王雪岩), Hu Wang(王虎), Luo-Ran Chen(陈烙然), Yu-Chuan Shao(邵宇川), and Jian-Da Shao(邵建达)
Chin. Phys. B, 2021, 30 (**11**): 118104. DOI: 10.1088/1674-1056/ac248d

Stability and optoelectronic property of low-dimensional organic tin bromide perovskites

J H Lei(雷军辉), Q Tang(汤琼), J He(何军), and M Q Cai(蔡孟秋)
Chin. Phys. B, 2021, 30 (**3**): 038102. DOI: 10.1088/1674-1056/abc545

Influences of nitrogen flow rate on the structures and properties of Ti and N co-doped diamond-like carbon films deposited by arc ion plating

Zhang Lin (张林), Ma Guo-Jia (马国佳), Lin Guo-Qiang (林国强), Ma He (马贺), Han Ke-Chang (韩克昌)
Chin. Phys. B, 2014, 23 (**4**): 048102. DOI: 10.1088/1674-1056/23/4/048102

RAPID COMMUNICATION

Stable photocurrent–voltage characteristics of perovskite single crystal detectors obtained by pulsed bias

Xin Liu(刘新)[1,2,3,†], Zhi-Long Chen(陈之龙)[1,3,4,†], Hu Wang(王虎)[1,2,3,‡], Wen-Qing Zhang(张雯清)[1,2,3], Hao Dong(董昊)[1,3,5], Peng-Xiang Wang(王鹏祥)[1,2,3], and Yu-Chuan Shao(邵宇川)[1,2,3,6,§]

[1] *Laboratory of Thin Film Optics, Shanghai Institute of Optics and Fine Mechanics, Chinese Academy of Sciences, Shanghai* 201800, *China*
[2] *Center of Materials Science and Optoelectronics Engineering, University of Chinese Academy of Sciences, Beijing* 100049, *China*
[3] *Key Laboratory of Materials for High-Power Laser, Shanghai Institute of Optics and Fine Mechanics, Chinese Academy of Sciences, Shanghai* 201800, *China*
[4] *Key Laboratory for Ultrafine Materials of Ministry of Education, Shanghai Engineering Research Center of Hierarchical Nanomaterials, School of Materials Science and Engineering, East China University of Science and Technology, Shanghai* 200237, *China*
[5] *School of Microelectronics, Shanghai University, Shanghai* 201899, *China*
[6] *Hangzhou Institute for Advanced Study, University of Chinese Academy of Sciences, Hangzhou* 310024, *China*

(Received 7 December 2023; revised manuscript received 3 January 2024; accepted manuscript online 30 January 2024)

Photocurrent–voltage characterization is a crucial method for assessing key parameters in x-ray or γ-ray semiconductor detectors, especially the carrier mobility lifetime product. However, the high biases during photocurrent measurements tend to cause severe ion migration, which can lead to the instability and inaccuracy of the test results. Given the mixed electronic–ionic characteristics, it is imperative to devise novel methods capable of precisely measuring photocurrent–voltage characteristics under high bias conditions, free from interference caused by ion migration. In this paper, pulsed bias is employed to explore the photocurrent–voltage characteristics of $MAPbBr_3$ single crystals. The method yields stable photocurrent–voltage characteristics at a pulsed bias of up to 30 V, proving to be effective in mitigating ion migration. Through fitting the modified Hecht equation, we determined the mobility lifetime products of 1.0×10^{-2} $cm^2\cdot V^{-1}$ for hole and 2.78×10^{-3} $cm^2\cdot V^{-1}$ for electron. This approach offers a promising solution for accurately measuring the transport properties of carriers in perovskite.

Keywords: perovskites, ion migration, pulsed bias, mobility lifetime product

PACS: 81.70.–q, 72.20.Jv, 81.05.Fb, 29.40.–n **DOI:** 10.1088/1674-1056/ad23d7

1. Introduction

Halide perovskite materials exhibit significant potential for application in optoelectronic devices.[1–4] It holds promise as a material of choice owing to its cost advantages and outstanding physical properties.[5–7] The transport characteristics of charge carriers are vital aspects of perovskite materials. Specifically, the carrier mobility lifetime product ($\mu\tau$) determines the performance and stability of semiconductor devices, where μ denotes the carrier mobility and τ is the carrier lifetime. Precise measurement of the carrier $\mu\tau$ is of utmost importance. Typically, the $\mu\tau$ can be obtained by strongly absorbing ionizing radiation, i.e., irradiating the sample with α-particles or γ-rays and investigating the charge collection efficiency.[8,9] Additionally, we can also determine $\mu\tau$ by visible light with energies surpassing the bandgap to stimulate carriers within the material, enabling the investigation of photocurrent–voltage properties.[10,11] To study the photocurrent–voltage characteristics of perovskites, it is necessary to gradually increase the bias voltage for a given light illumination with the aim of saturating the photocurrent.[12,13] This requires the material to exhibit excellent stability under high bias conditions.

Traditionally, direct current bias is the prevailing choice for electrical measurements. Nevertheless, in the case of halide perovskites, the conventional approach to determining $\mu\tau$ involved assessing the photocurrent–voltage characteristics under direct current bias. However, noteworthy photocurrent drift occurs at elevated direct current bias levels. Consequently, while the conventional method can capture the photocurrent trend with voltage, the resulting $\mu\tau$ values lack accuracy. For example, in the prototypical $MAPbBr_3$ single crystals (SCs), both dark and light currents exhibit instability beyond direct current bias levels of about 2–5 V. This is because the lattice of perovskite materials exhibits relative softness, leading to the gradual severity of ion migration with increasing voltage.[14,15] Additionally, defects within the material can serve as channels for ion migration.[16,17]

Previous studies have demonstrated that ion migration can be effectively mitigated through the use of pulsed voltage. For instance, employing pulsed voltage along with space

[†]These authors contributed equally to this work.
[‡]Corresponding author. E-mail: wanghu@siom.ac.cn
[§]Corresponding author. E-mail: shaoyuchuan@siom.ac.cn

© 2024 Chinese Physical Society and IOP Publishing Ltd

charge limited current accurately determines the defect density and mobility of carriers.[18–20] Additionally, the combination of pulsed voltage and the time-of-flight method enables precise measurement of carrier mobility in perovskite SCs.[21,22] Take advantage of pulsed bias in inhibiting ion migration, minimal dark current drift can be achieved.[23] Nevertheless, it's rarely reported on pulsed bias to enhance the stability of photocurrent.

In this study, we employed both direct current bias and pulsed bias to investigate the photocurrent–voltage characteristics of $MAPbBr_3$ SCs, aiming to enhance our understanding of the carrier transport properties in perovskite detectors. Under pulsed bias conditions, up to 30 V, both dark and light currents exhibit notable stability, confirming the effectiveness of pulsed voltage inhibition of ion migration. With the pulsed bias mode, we obtained stable photocurrent–voltage characteristics. The $\mu\tau$ for the hole in $MAPbBr_3$ was determined to be approximately 1.0×10^{-2} $cm^2\cdot V^{-1}$ and for the electron, it was around 2.78×10^{-3} $cm^2\cdot V^{-1}$ through fitting with the modified Hecht equation.[24,25] This study presents a new approach to understanding the current–voltage behavior of perovskite materials, enhancing the stability of investigating carrier transport properties.

2. Experiments

Synthesis of $MAPbBr_3$ single crystals The modified inverse temperature crystal growth (ITC) method was employed to cultivate $MAPbBr_3$ SCs.[26] Methyl ammonium bromide (MABr, 99.5%) was purchased from Xi'an Spotlight Technology Co. Lead bromide ($PbBr_2$, 99%) was purchased from Aladdin Regent Ltd. N,N-dimethylformamide (DMF, 99.9%) was purchased from Sigma Aldrich. Added 0.3359 g of MABr and 1.1010 g of $PbBr_2$ to 2 ml of DMF solvent and stirred in a 20 ml glass vial for 6 hours. Afterwards, the precursor solution was filtered through a 0.22 μm polytetrafluoroethylene filter. The solution was then heated on a hot table from 40 °C to 60 °C and finally kept at 60 °C for crystal growth. Finally, SCs with a thickness of about 2 mm and a size of 4–8 mm were obtained.

Material characterization The bulk $MAPbBr_3$ SC was crushed into powder using mortar and pestle. Powder XRD was performed by using an x-ray diffractometer (PANalytical Empyrean) with Cu $K\alpha$ radiation. High-resolution x-ray diffraction (XRD) rocking curves were acquired employing an x-ray diffractometer (Bruker D8-Discover). Photoluminescence (PL) and time-resolved photoluminescence spectra (TRPL) were captured at room temperature using a laser-scanning fluorescence lifetime/intensity imaging system (FLRM, Time-Tech Spectra, LLC) with a laser intensity of 1.48 μW and a 405 nm picosecond pulsed diode laser serving as the excitation source.

Device fabrication Metal electrodes were thermally vapor-deposited onto the surfaces of SCs. In the case of horizontal devices, 25 nm of C60, 10 nm of BCP, and 40 nm of Au were successively deposited on the surface of the 7 mm×7 mm×2 mm $MAPbBr_3$ SC using a shadow mask (Au/BCP/C60/$MAPbBr_3$/C60/BCP/Au). Alternatively, 40 nm of Au was deposited on the same surface of the $MAPbBr_3$ SC using the same method (Au/$MAPbBr_3$/Au). The channel spacing was 0.2 mm. For vertically structured devices, 25 nm of C60, 10 nm of BCP, and 40 nm of Au were sequentially deposited on both sides of the 5 mm×5 mm×2 mm $MAPbBr_3$ SC (Au/BCP/C60/$MAPbBr_3$/C60/BCP/Au). Alternatively, 40 nm of Au was deposited on both sides of the $MAPbBr_3$ SC (Au/$MAPbBr_3$/Au). The Schottky structure (Au/$MAPbBr_3$/C60/BCP/Au) was created by depositing 40 nm of Au on one side of the $MAPbBr_3$ SC. On the other side, 25 nm of C60, 10 nm of BCP, and 40 nm of Au were deposited sequentially. The effective area of the vertical device electrodes was 3 mm×3 mm.

Device measurement The current density–voltage (I–V) curves were recorded using the Keithley 2634B source meter. Photocurrent–voltage characteristics were assessed under the illumination of a 520 nm green LED, with the device enclosed in a lead box for measurements. Pulsed light, controlled by the Keysight 33500B signal generator, illuminated the device with a peak-to-peak value of 3 V and a period denoted as T. The optical power of the LED was measured to be about 40 μW with an optical power meter. A small aperture diaphragm was added directly between the LED and the device to be measured to focus the beam. By switching visible light on and off, the output light current and dark current curves can be obtained with the Keithley 2634B. And the photocurrent–voltage characteristic can be obtained by photocurrent = light current − dark current. The Keithley 2634B source meter supplied the bias for the perovskite device. In the pulsed bias mode, the voltage duration was t_1 and the waiting interval was t_2.

3. Results and discussion

The measurement system employed for photocurrent–voltage characterization in direct current bias mode is shown in Fig. 1(a), which provides a sustained voltage to the device over an extended period. Direct current voltage is a widely used method of electrical measurement. The testing apparatus comprises multiple components. A source meter connects to a perovskite detector, serving as a voltage source for the direct current bias applied to the detector, and as a current source for measuring the output current of the sample under examination. The signal generator applies a pulsed bias with a 50% duty cycle to the green LED, facilitating pulsed visible light

irradiation onto the perovskite detector's surface. It is imperative to note that, for the excitation of photogenerated carriers, the photon energy of the light source must surpass the bandgap of the tested perovskite material, i.e., $h\omega > E_g$. The period of the visible light is denoted as T. Our investigation involves the study of photocurrent at various biases, where photocurrent is defined as the difference between light current and dark current. Given the pulsed nature of the applied light, we can directly acquire light current and dark current from the current source connected to the computer, enabling the calculation of the difference to determine the photocurrent.

Nevertheless, in the direct current bias mode, the light and dark currents exhibit increasing instability as the voltage rises,[27] as illustrated by the gradual drift in Fig. 1(b). This phenomenon contributes to the development of a measurement history, significantly impacting subsequent electrical measurements and necessitating an extended recovery time. Consequently, the photocurrent–voltage characteristics obtained under these conditions are notably inaccurate due to ion migration within the perovskite SCs.

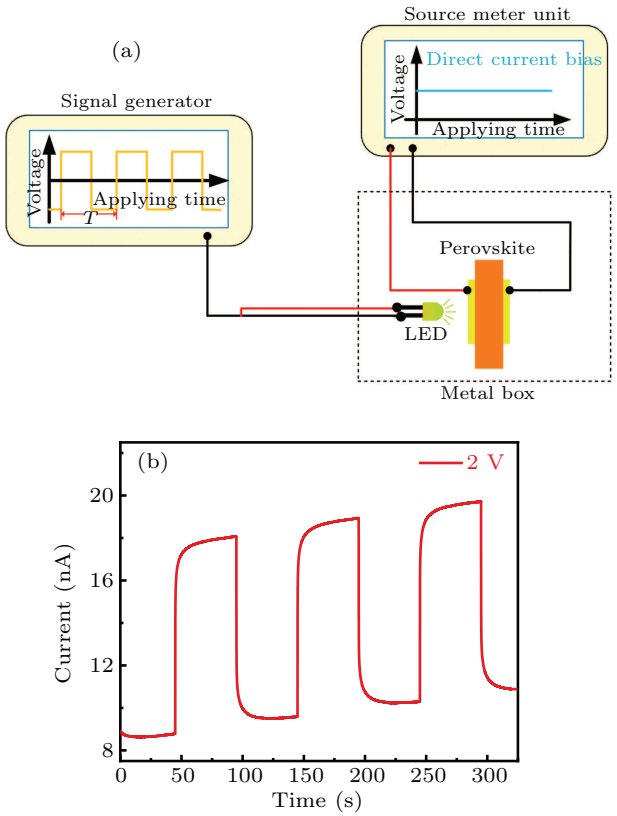


Fig. 1. (a) Schematic diagram illustrating the photocurrent–voltage characteristics measurement system of perovskite SC detectors in direct current bias mode. (b) Visible light on–off curve of $MAPbBr_3$ SC detector at 2 V direct current bias with drift in photocurrent and dark current.

The perovskite material exhibits a general formula ABX_3, where A^+ represents organic amine cations (MA^+, FA^+) or inorganic cations (Cs^+), B^{2+} denotes Pb^{2+} and other metal ions, and X^- stands for halogen anions such as Cl^-, Br^-, I^-, etc.[28] Prolonged direct current bias induces significant migration of ions at the A^+ and X^- sites within the perovskite structure, as depicted in Fig. 2(a). Conversely, migration of A^+ and X^- within the perovskite material under pulsed bias is essentially negligible. This method has proven effective in suppressing ion migration within the crystal, thereby mitigating the dark current drift.

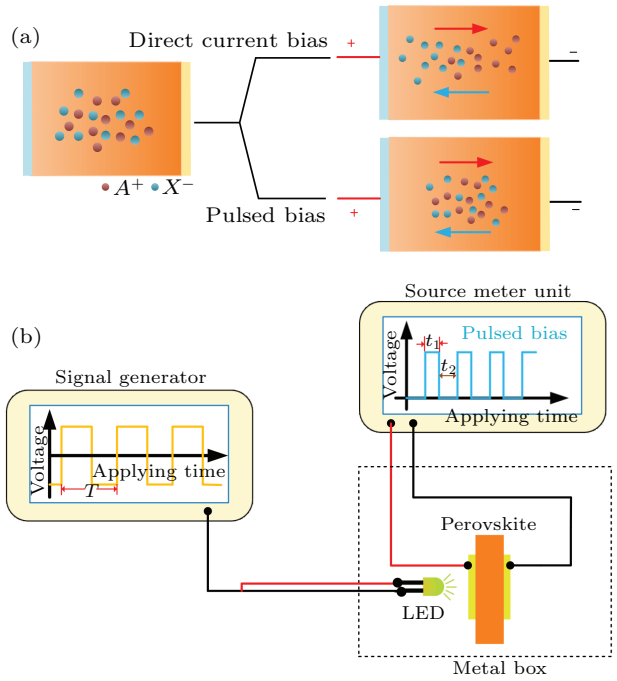


Fig. 2. (a) Investigation of ion migration within the perovskite material under two operational modes: direct current bias and pulsed bias. (b) Schematic diagram illustrating the measurement system for photocurrent–voltage characteristics of perovskite SC detectors in pulsed bias mode.

Therefore, we examined the photocurrent–voltage characteristics under pulsed bias conditions, and the measurement system is depicted in Fig. 2(b). In contrast to the direct current bias mode, the source meter delivers a pulsed voltage signal to the detector. The output parameters governing the source meter include the magnitude of the pulsed bias, the voltage duration t_1, the waiting interval t_2, and so forth. The combination of t_1 and t_2 constitutes one cycle of the pulsed bias voltage. Employing this method allows for ample waiting time, where the voltage duration t_1 is 50 ms, and the waiting interval t_2 is on the order of 1 s or more. The parameters of the other measuring devices are consistent with those of the devices in the direct current bias mode, e.g., the parameters of the LED. In this mode, the optical period T must significantly exceed the sum of t_1 and t_2, about 50 times longer. The specific parameters of the pulsed bias mode in our work are shown in Table S1, and the schematic time sequence of pulse voltage and LED is shown in Fig. S1. The increase in bias voltage leads to more severe ion migration and greater drift in both right and dark currents. To effectively suppress ion migration, it is therefore necessary to increase the waiting interval t_2 during

the measurement depending on the voltage increase. We have investigated different waiting intervals at different voltages as shown in Figs. S2–S5. For example, when the bias voltage to which the vertical device is subjected is greater than 10 V. In order to achieve the T much longer than the sum of t_1 and t_2, we need to simultaneously extend the LED period T. This approach provides sufficient recovery time for the ions in the perovskite materials so that we can obtain stability at higher bias voltages.

In our research, we employed $MAPbBr_3$ SCs as the standard organic–inorganic hybridized perovskite, measuring approximately 5 mm×5 mm (Fig. 3(a)). The quality of the SCs was assessed before the photoelectric measurements. The phase purity of the $MAPbBr_3$ SC is confirmed according to the powder XRD pattern (Fig. S6). The high-resolution XRD rocking curve of the SC yields a half-peak full width at half maximum (FWHM) of 0.018° (Fig. 3(b)). The luminescence properties of $MAPbBr_3$ SCs were measured prior to fabricating the perovskite devices. The PL spectra of the recently prepared SCs exhibit a peak at 542 nm (Fig. 3(c)), and TRPL indicates a fluorescence lifetime of 35.64 ns (Fig. 3(d)). These characterizations affirm the high quality of our SCs.

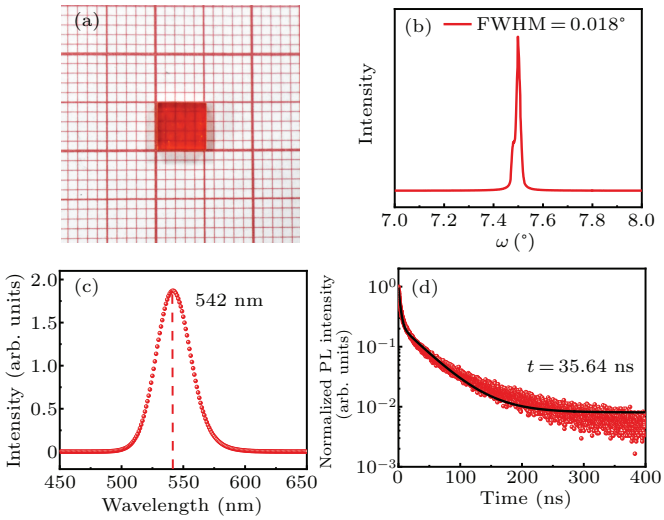


Fig. 3. Characterization of $MAPbBr_3$ SCs. (a) Photographs of fresh $MAPbBr_3$ SC of 5 mm×5 mm×2 mm. (b) High-resolution x-ray diffraction rocking curves of $MAPbBr_3$ SC at (100) peak. (c) PL spectra and (d) TRPL spectra of $MAPbBr_3$ SC.

Initially, we examined both light and dark currents under direct current bias and pulsed bias modes on horizontal devices. The horizontal device structure schematic is shown in Figs. S7(a) and S7(b). The results are the current curves for visible light on–off as shown in Fig. 4. The electrode channel distance in the horizontal device is merely 0.2 mm, resulting in a stronger electric field. In the pulsed bias mode, the parameters for voltage are set as follows: $t_1 = 50$ ms, $t_2 = 1$ s. The period T of LED light remains constant at 100 s in both bias modes. In the $Au/MAPbBr_3/Au$ device, the light and dark currents exhibit drift at 0.5 V in direct current bias mode, with a pronounced drift occurring at 3 V (Fig. 4(a)). The extent of drift in both light and dark currents increases with rising direct current bias, signifying that prolonged application of direct current bias will notably impact carrier transport. Under pulsed bias mode, both light and dark currents remain highly stable from 0.5 V to 3 V with minimal drift (Fig. 4(b)).

In the $Au/BCP/C60/MAPbBr_3/C60/BCP/Au$ devices, slight instability is observed in both light and dark currents at 3 V in direct current bias mode, with the light current becoming significantly unstable at direct current voltages up to 7 V (Fig. 4(c)). Conversely, the light and dark currents of the $MAPbBr_3$ detector remain stable under pulsed bias from 1 V to 7 V (Fig. 4(d)). The effectiveness of pulsed bias was demonstrated for horizontal devices with different electrode materials. Compared with direct current bias, pulsed bias effectively suppresses ion migration, thus preventing light and dark currents drift.

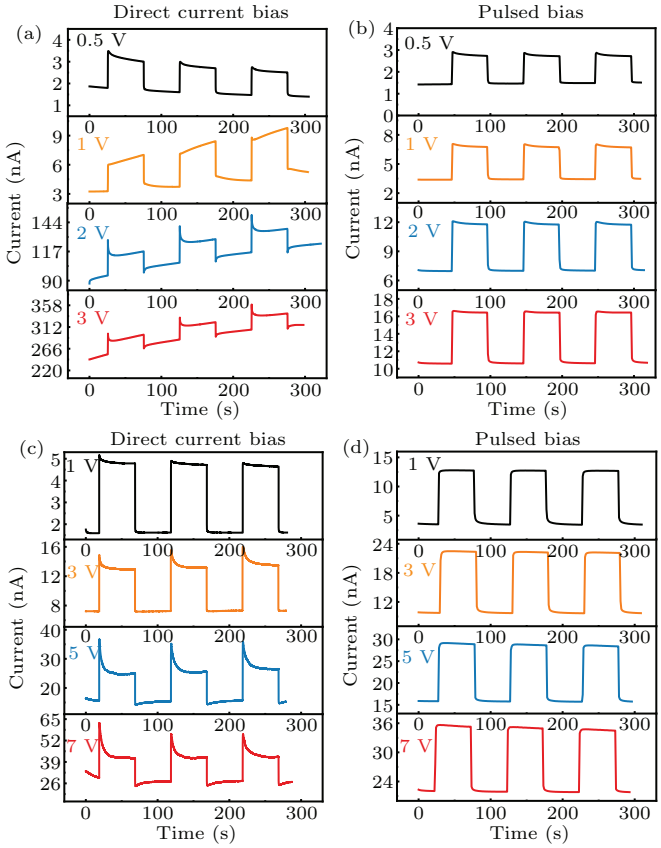


Fig. 4. (a), (b) Visible light on–off curves of $MAPbBr_3$ SC detector with $Au/MAPbBr_3/Au$ horizontal structure under various direct current biases and pulsed biases. (c), (d) Visible light on–off curves of $MAPbBr_3$ SC detector with $Au/BCP/C60/MAPbBr_3/C60/BCP/Au$ horizontal structure under various direct current biases and pulsed biases.

Then we explored visible light on–off curves in direct current bias and pulsed bias modes on vertical devices, the structure of which is shown in Figs. S7(c) and S7(d). In the $Au/MAPbBr_3/Au$ device, the light current exhibits drift at 1 V direct current bias and substantial drift at 4 V (Fig. 5(a)). Under pulsed bias mode, both light and dark currents remain highly stable from 1 V to 30 V with minimal drift (Fig. 5(b)).

In the Au/BCP/C60/$MAPbBr_3$/C60/BCP/Au devices, the light current exhibits instability at direct current voltages ranging from about 3 V to 8 V (Fig. 5(c)). However, as depicted in Fig. 5(d), the light and dark currents of the $MAPbBr_3$ detector remain stable at pulsed bias up to 30 V. The results from the vertical device align with those of the horizontal device, suggesting that the pulsed bias mode can achieve stable light and dark currents at high voltages, in contrast to the direct current bias mode. The effectiveness of pulsed bias in inhibiting ion migration in $MAPbBr_3$ detectors with diverse device structures is confirmed.

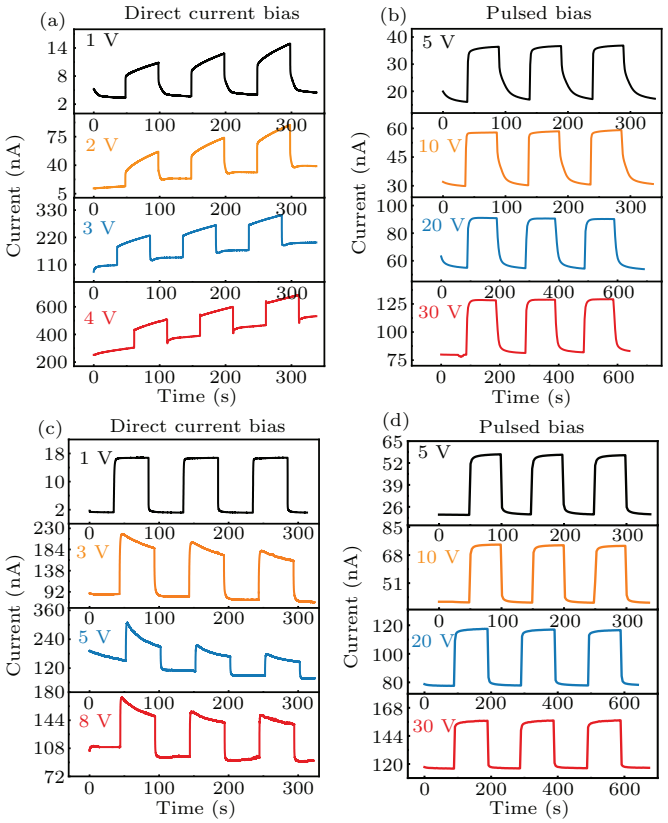


Fig. 5. (a), (b) Visible light on–off curves of $MAPbBr_3$ SC detector with Au/$MAPbBr_3$/Au vertical structure under various direct current biases and pulsed biases. (c), (d) Visible light on–off curves of $MAPbBr_3$ SC detector with Au/BCP/C60/$MAPbBr_3$/C60/BCP/Au horizontal structure under various direct current biases and pulsed biases.

Since the Schottky structure suppresses carrier injection and dark current, so we conducted a thorough investigation into the photocurrent–voltage characteristics of Au/$MAPbBr_3$/C60/BCP/Au with the Schottky structure depicted in Fig. 6(a). Initially, we examined the *I*–*V* hysteresis of the $MAPbBr_3$ detector in the dark under two different voltages using the source meter (Fig. 6(b)).[29–31] The hysteresis width is significantly diminished in pulsed voltage compared to the direct current voltage. Light is directed onto the cathode to acquire hole transport characteristics. Both light and dark currents exhibit substantial drift at a direct current bias of approximately 4 V (Fig. 6(c)). Conversely, under a high pulsed bias of 30 V, the light and dark currents remain stable with minimal drift (Fig. 6(d)). By increasing the waiting time t_2 we can also obtain stable visible on–off curves at higher bias voltages, such as 60 V in Fig. S4 and 100 V in Fig. S5. The relationship between photocurrent and voltage is derived from the disparity between light current and dark current, as depicted in Fig. 6(e). The calculation is performed using the enhanced Hecht equation

$$I = \frac{I_0 \mu \tau U}{L^2}\left[\frac{1-\mathrm{e}^{-\frac{L^2}{\mu\tau U}}}{1+\frac{Ls}{U\mu}}\right], \tag{1}$$

where I_0 represents the photocurrent saturation value, L denotes the crystal thickness, and U stands for the bias. The equation assumes the absence of space charge in the sample at rest, a uniform internal electric field, and a division of carriers generated by illumination: some drift under the external electric field, while others undergo recombination at the surface. Consequently, the $\mu\tau$ for the hole in $MAPbBr_3$ is deduced to be approximately 1.0×10^{-2} $cm^2{\cdot}V^{-1}$ and that of the electron is about 2.78×10^{-3} $cm^2{\cdot}V^{-1}$. They are in the same order of magnitude compared to previous reports, as shown in Table S2.

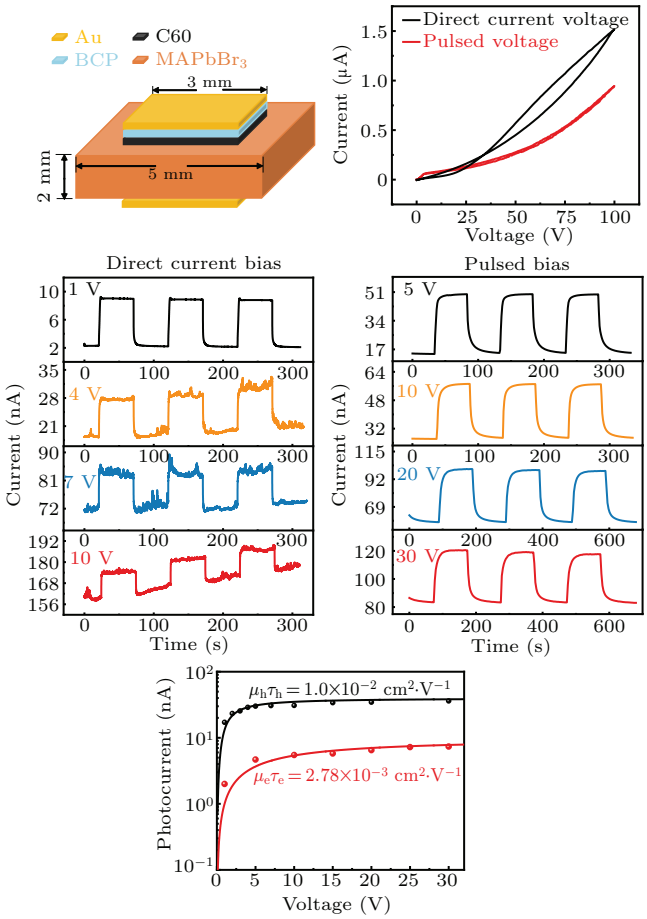


Fig. 6. (a) Schematic device structure of Au/$MAPbBr_3$/C60/BCP/Au. (b) Current hysteresis at direct current voltage and pulse voltage. (c), (d) Visible light on–off curves of $MAPbBr_3$ SC detector with Au/BCP/C60/$MAPbBr_3$/C60/BCP/Au horizontal structure under various direct current biases and pulsed biases. (e) Photocurrent–voltage characteristics curve of $MAPbBr_3$ SC detector. Dots are experimental data and lines are fitted values.

4. Conclusion and outlook

In conclusion, we investigated the photocurrent–voltage characteristics of $MAPbBr_3$ SC detectors, employing both direct current bias and pulsed bias. By comparing $MAPbBr_3$ single-crystal detectors with varying device structures and electrode materials, we proved that pulsed bias effectively mitigates both dark and photocurrent drift. Under direct current bias mode at approximately 5 V, the $MAPbBr_3$ single-crystal detector experiences significant photocurrent drift. In contrast, under pulsed bias, the photocurrent remains stabilized even up to 30 V. This is attributed to the suppression of ion migration within the perovskite SCs in pulsed bias mode, as opposed to direct current bias. This suppression is evident in the attainment of stable light and dark currents. We obtained the stable photocurrent–voltage characteristics of the $MAPbBr_3$ SC detector and derived the saturation photocurrent curve. The hole mobility lifetime product $\mu_h\tau_h$ was calculated to be approximately 1.0×10^{-2} $cm^2\cdot V^{-1}$, and the corresponding value for electron $\mu_e\tau_e$ is around 2.78×10^{-3} $cm^2\cdot V^{-1}$. This study verifies the accurate and stable measurement of photocurrent–voltage characteristics in perovskite single-crystal detectors through the utilization of pulsed bias. Additionally, it offers novel insights into the carrier transport properties of halide perovskites.

Acknowledgements

Project supported by the National Natural Science Foundation of China (Grant No. 62104234) and Shanghai Explorer Program (Grant No. 22TS1400100).

References

[1] Yang Z Q, Deng Y H, Zhang X W, Wang S, Chen H Z, Yang S, Khurgin J, Fang N X, Zhang X and Ma R 2018 *Adv. Mater.* **30** 1704333
[2] Li N X, Tao S X, Chen Y H, *et al*. 2019 *Nat. Energy* **4** 408
[3] Jeong J, Kim M, Seo J, *et al*. 2021 *Nature* **592** 381
[4] Li G X, Su Z H, Canil L, *et al*. 2023 *Science* **379** 399
[5] Wei H T and Huang J S 2019 *Nat. Commun.* **10** 1066
[6] Lin R X, Wang Y R, Lu Q W, Tang B B, Li J Y, Gao H, Gao Y, Li H J, Ding C Z, Wen J, Wu P, Liu C S Y, Zhao S Y, Xiao K, Liu Z, Ma C Q, Deng Y, Li L D, Fan F J and Tan H R 2023 *Nature* **620** 994
[7] Zhao Y J, Yin X, Li P W, Ren Z Q, Gu Z K, Zhang Y Q and Song Y L 2023 *Nano-Micro Lett.* **15** 187
[8] He Y H, Petryk M, Liu Z F, Chica D G, Hadar I, Leak C, Ke W J, Spanopoulos I, Lin W W, Chung D Y, Wessels B W, He Z and Kanatzidis M G 2021 *Nat. Photon.* **15** 36
[9] Klepov V V, De Siena M C, Pandey I R, Pan L, Bayikadi K S, Butun S, Chung D Y and Kanatzidis M G 2023 *ACS Appl. Mater. Interfaces* **15** 16895
[10] Cui Y, Wright G W, Ma X, Chattopadhyay K, James R B and Burger A 2001 *J. Electron. Mater.* **30** 774
[11] Cui Y, Groza M, Hillman D, Burger A and James R B 2002 *J. Appl. Phys.* **92** 2556
[12] Ling Y P, Min J H, Liang X Y, Zhang J J, Yang L Q, Zhang Y, Li M, Liu Z X and Wang L J 2017 *J. Appl. Phys.* **121** 034502
[13] Ridzonova K, Belas E, Grill R, Pekarek J and Praus P 2020 *Phys. Rev. Appl.* **13** 064054
[14] Xiao Z G, Yuan Y B, Shao Y C, Wang Q, Dong Q F, Bi C, Sharma P, Gruverman A and Huang J S 2015 *Nat. Mater* **14** 193
[15] Zhang Y P, Wang Y S, Xu Z Q, Liu J Y, Song J C, Xue Y Z, Wang Z Y, Zheng J L, Jiang L C, Zheng C X, Huang F Z, Sun B Q, Cheng Y B and Bao Q L 2016 *ACS Nano* **10** 7031
[16] Shao Y C, Fang Y J, Li T, Wang Q, Dong Q F, Deng Y H, Yuan Y B, Wei H T, Wang M Y, Gruverman A, Shield J and Huang J S 2016 *Energy Environ. Sci.* **9** 1752
[17] Azpiroz J M, Mosconi E, Bisquert J and Angelis D F 2015 *Energy Environ. Sci.* **8** 2118
[18] Duijnstee E A, Ball J M, Le Corre V M, Koster L J A, Snaith H J and Lim J 2020 *ACS Energy Lett.* **5** 376
[19] Le Corre V M, Duijnstee E A, Tambouli O E, Ball J M, Snaith H J, Lim J and Koster L J A 2021 *ACS Energy Lett.* **6** 1087
[20] Duijnstee E A, Le Corre V M, Johnston M B, Koster L J A, Lim J and Snaith H J 2021 *Phys. Rev. Appl.* **15** 014006
[21] Musiienko A, Ceratti D R, Pipek J, Brynza M, Elhadidy H, Belas E, Betušiak M, Delport G and Praus P 2021 *Adv. Funct. Mater.* **31** 2104467
[22] Qin J, Cao G, Xu R, Lin J, Meng H, Wang W Z, Hong Z Y, Cai J C, and Li D M 2022 *Chin. Phys. B* **31** 117102
[23] Wang X Y, Wang H, Chen L R, Shao Y C, and Shao J D 2021 *Chin. Phys. B* **30** 118104
[24] Hecht K 1932 *Z. Physik* **77** 235
[25] Many A 1965 *J. Phys. Chem. Solids* **26** 575
[26] Saidaminov M I, Abdelhady A L, Murali B, Alarousu E, Burlakov V M, Peng W, Dursun I, Wang L F, He Y, Maculan G, Goriely A, Wu T, Mohammed O F and Bakr O M 2015 *Nat. Commun.* **6** 7586
[27] Tayagaki T, Kogo A, McDonald C, Svrcek V, Matsui T and Yoshita M 2022 *IEEE J. Photovolt.* **12** 1170
[28] Jena A K, Kulkarni A and Miyasaka T 2019 *Chem. Rev.* **119** 3036
[29] Zhang T, Chen H N, Bai Y, Xiao S, Zhu L, Hu C, Xue Q Z and Yang S H 2016 *Nano Energy* **26** 620
[30] Khassaf H, Yadavalli S K, Game O S, Zhou Y Y, Padture N P and Kingon A I 2019 *J. Phys. Chem. C* **123** 4029
[31] Cave J M, Courtier N E, Blakborn I A, Jones T W, Ghosh D, Anderson K F, Lin L Y, Dijkhoff A A, Wilson G J, Feron K, Saiful Islam M, Foster J M, Richardson G and Walker A B 2020 *J. Appl. Phys.* **128** 184501